arXiv:1407.1244v2 [cond-mat.mes-hall] 22 Sep 2014

Spin-orbit spillage as a measure of band inversion in insulators

Jianpeng Liu[1] and David Vanderbilt[1]

[1]*Department of Physics and Astronomy, Rutgers University, Piscataway, NJ 08854-8019, USA*

(Dated: September 23, 2014)

We propose a straightforward and effective approach for quantifying the band inversion induced by spin-orbit coupling in band insulators. In this approach we define a quantity as a function of wavevector in the Brillouin zone measuring the mismatch, or "spillage", between the occupied states of a system with and without SOC. Plots of the spillage throughout the BZ provide a ready indication of the number and location of band inversions driven by SOC. To illustrate the method, we apply this approach to the two-band Dirac model, the 2D Kane-Mele model, a 2D Bi bilayer with applied Zeeman field, and to first-principles calculations of some 3D materials including both trivial and $\mathbb{Z}_2$ topological insulators. We argue that the distribution of spillage in the BZ is closely related to the topological indices in these systems. Our approach provides a fresh perspective for understanding topological character in band theory, and should be helpful in searching for new materials with non-trivial band topology.

PACS numbers: 71.70.Ej, 03.65.Vf

I. INTRODUCTION

Spin-orbit coupling (SOC) is a relativistic effect originating from the interaction between the spin and orbital motions of electrons. It has played a key role in various aspects of condensed-matter physics, including the electronic structure of solids and the transport properties in mesoscopic systems.[1,2] It has been known since the 1950s that SOC can induce anisotropic spin splitting in some III-V semiconductors with the zinc-blende structure, known as the Dresselhaus splitting.[1] In 2D and quasi-2D systems, the SOC resulting from the electric field perpendicular to the 2D plane gives rise to a Rashba splitting linear in k with interesting "helical" spin textures.[1,2] The SOC is also crucial in determining the transport behavior of low-dimensional electronic systems. One famous example is the weak antilocalization in spin-orbit-coupled 2D electronic systems, where the backscattering amplitudes interfere destructively due to a geometric Berry phase[3] associated with the intrinsic SOC, leading to a suppressed resistivity when an external magnetic field is absent.[4] SOC is also responsible for spin precession in 1D and quasi-1D systems,[2] the spin Hall effect in paramagnetic metals,[5] and numerous other effects.

The SOC has received renewed attention recently because of its central role in the physics of topological insulators (TIs) and related topological states. Typically, the transition from a topologically trivial to a non-trivial phase is accomplished by a SOC-driven inversion of states of different symmetry at the conduction-band minimum (CBM) and valence-band maximum (VBM). For example, such a SOC-driven topological band inversion between Γ_6-derived (s-like) and Γ_8-derived (p-like) states at the zone center is responsible for the quantum spin Hall (QSH) state observed in HgTe/CdTe quantum wells.[6,7] Similarly, the Kane-Mele model of 2D graphene-like systems[8,9] enters the QSH state when two band inversions occur at the K and K$'$ points as the SOC strength is increased at a constant staggered potential. In 3D band insulators with time-reversal (TR) symmetry, a SOC-induced band inversion can transform the system from a trivial insulator into a strong TI displaying an odd number of gapless Dirac cones in the surface states, as occurs for Bi_2Se_3 and Bi_2Te_3.[10–13]

In the case of a 3D strong TI with inversion symmetry such as Bi_2Se_3, the strong $\mathbb{Z}_2$ index can be uniquely determined by the parities of the occupied bands at the TR-invariant momenta (TRIM) in the Brillouin zone (BZ).[14] If the highest occupied states and lowest unoccupied states at one of the TRIM possess opposite parities without SOC, and they are inverted by turning on SOC, then the system transforms from a normal to a topological insulator. For example, in Bi_2Se_3, two pairs of Kramers-degenerate occupied states at the BZ center (Γ) are inverted by SOC, resulting in the nontrivial $\mathbb{Z}_2$ index. For TIs without inversion symmetry, the band inversion may happen at arbitrary points in the BZ, instead of at the TRIM. We can identify such band inversion points as the points where a band touching occurs between valence and conduction bands as the SOC is adiabatically turned on; TR symmetry implies that an inversion at $\mathbf{k}_0$ will always be accompanied by one at $-\mathbf{k}_0$. Even in the absence of inversion symmetry, therefore, a band inversion driven by SOC is typically a hallmark of the non-trivial topology in TIs with TR symmetry.

The SOC also plays a crucial role in giving rise to the Chern insulator (CI) state, also known as the quantum anomalous Hall state, which can occur in 2D insulators lacking time-reversal symmetry. The possibility of a CI state was first introduced by Haldane,[15] who constructed an explicit model that demonstrates the effect. Although the Haldane model is a model of spinless Fermions on a honeycomb lattice, its key feature is the presence of complex second-neighbor hoppings, which can be regarded as arising from intrinsic atomic SOC through a second-order perturbation process in a more realistic system of spinor electrons.[16] An example is a Bi bilayer with an applied Zeeman field, as will be discussed below.

The concept of topological band inversion has been much discussed in the topological-insulator literature, but in the absence of symmetry it may be difficult to recognize when a band inversion has actually occurred. The usual approach is to look at the symmetry or orbital character at a high-symmetry point in the BZ where a band inversion is suspected, but this only works if sufficient symmetry is present. Some authors have tried to deduce the presence of band-inversion behav-

ior by studying other properties of the system, such as by looking at the qualitative shape of the bands near the symmetry point,[17] or even more indirectly, by studying the variation of the band-energy differences with strain in the absence of SOC.[18] However, the reliability of such methods is questionable, as they do not give a direct and quantitative evaluation of the SOC-induced band inversion.

In this paper, we propose that the calculation of spin-orbit spillage, which measures the degree of mismatch between the occupied band projection operators with and without SOC, provides a simple and effective measure of SOC-driven band inversion in insulators. We demonstrate that the mapping of this spin-orbit spillage in k-space easily allows a direct identification of any region in the BZ where band inversion has occurred, and that the maximum spillage is a useful indicator of topological character. We illustrate the method in the context of both tight-binding models and realistic first-principles calculations.

The paper is organized as follows. In Sec. II the formal definition of SOC-induced spillage is introduced, and the correspondence between topological indices and spillage is also discussed. In Sec. III the formalism is applied to various systems, including the two-band Dirac model, 2D Kane-Mele model, a Bi bilayer with tunable SOC and exchange field, and realistic materials including Bi_2Se_3, In_2Se_3, and Sb_2Se_3. In Sec. IV we make a brief summary.

II. FORMALISM

A. Definitions

Mathematically, the mismatch between two projection operators P and $\widetilde{P}$, both of rank N, can be represented by a quantity

$$\gamma = N - \mathrm{Tr}[P\widetilde{P}] = \mathrm{Tr}[P\widetilde{Q}] = \mathrm{Tr}[Q\widetilde{P}] \tag{1}$$

where $Q = 1 - P$ and $\widetilde{Q} = 1 - \widetilde{P}$ denote the complementary projections. This measure of mismatch is often referred to as "spillage" since it measures the weight of states that spill from P into $\widetilde{Q}$, or equivalently, from $\widetilde{P}$ into Q. Clearly the spillage vanishes if $P = \widetilde{P}$ at one extreme, and rises to N at the other extreme if there is no overlap at all between the subspaces associated with P and $\widetilde{P}$. Thus, the spillage provides a measure of the degree of mismatch between the two subspaces.

Here we apply this concept to the band projection operators

$$P(\mathbf{k}) = \sum_{n=1}^{n_{\mathrm{occ}}} |\psi_{n\mathbf{k}}\rangle\langle\psi_{n\mathbf{k}}| \tag{2}$$

associated with a given wavevector $\mathbf{k}$ in the BZ of a crystalline insulator with $N = n_{\mathrm{occ}}$ occupied bands. We assume an effective single-particle Hamiltonian such as that appearing in density-functional theory (DFT).[19,20] Then the SOC-induced spillage $\gamma(\mathbf{k})$ is defined as

$$\gamma(\mathbf{k}) = \mathrm{Tr}[P(\mathbf{k})\widetilde{Q}(\mathbf{k})] \tag{3}$$

where P and $\widetilde{P}$ (and their complements) refer to the system with and without SOC respectively. More explicitly,

$$\begin{aligned}\gamma(\mathbf{k}) &= n_{\mathrm{occ}} - \mathrm{Tr}[P(\mathbf{k})\widetilde{P}(\mathbf{k})] \\ &= n_{\mathrm{occ}} - \sum_{m,n=1}^{n_{\mathrm{occ}}} |M_{mn}(\mathbf{k})|^2\end{aligned} \tag{4}$$

where

$$M_{mn}(\mathbf{k}) = \langle\psi_{m\mathbf{k}}|\tilde{\psi}_{n\mathbf{k}}\rangle \tag{5}$$

is the overlap between occupied Bloch functions with and without SOC at the same wavevector $\mathbf{k}$. Equivalently, this can be written as $M_{mn}(\mathbf{k}) = \langle u_{m\mathbf{k}}|\tilde{u}_{n\mathbf{k}}\rangle$ if one prefers to work in terms of the cell-periodic $|u_{n\mathbf{k}}\rangle$ defined as $u_{n\mathbf{k}}(\mathbf{r}) = e^{-i\mathbf{k}\cdot\mathbf{r}}\psi_{n\mathbf{k}}(\mathbf{r})$.

In the case of realistic DFT calculations in a plane-wave basis, the overlap matrix elements are easily evaluated as

$$M_{mn}(\mathbf{k}) = \sum_{\mathbf{G}} \langle\psi_{m\mathbf{k}}|\mathbf{k}+\mathbf{G}\rangle\langle\mathbf{k}+\mathbf{G}|\tilde{\psi}_{n\mathbf{k}}\rangle\,, \tag{6}$$

where $|\mathbf{k}+\mathbf{G}\rangle$ is the plane wave $e^{i(\mathbf{k}+\mathbf{G})\cdot\mathbf{r}}$ for reciprocal vector $\mathbf{G}$ normalized to the unit cell. The evaluation should also be straightforward in other first-principles basis sets. For simple lattice models the Hamiltonian is typically written in an orthonormal tight-binding basis, so that the wavefunctions are

$$|\psi_{n\mathbf{k}}\rangle = \sum_j C_{nj,\mathbf{k}}\,|\chi_{j\mathbf{k}}\rangle \tag{7}$$

where $|\chi_{j\mathbf{k}}\rangle$ are the Bloch basis states

$$\chi_{j\mathbf{k}}(\mathbf{r}) = \sum_{\mathbf{R}} e^{i\mathbf{k}\cdot\mathbf{R}}\,\varphi_j(\mathbf{r}-\mathbf{R}) \tag{8}$$

and $\varphi_j(\mathbf{r}-\mathbf{R})$ is the j'th tight-binding basis orbital in unit cell $\mathbf{R}$. Then the spillage is trivially computed using

$$M_{mn}(\mathbf{k}) = \sum_j C^*_{mj,\mathbf{k}}\widetilde{C}_{nj,\mathbf{k}}\,. \tag{9}$$

Since the use of Wannier interpolation methods[21–23] is becoming increasingly frequent, we also comment on this case here. In this approach, the occupied Bloch states are again written as in Eq. (7), but this time the Bloch basis states are

$$\chi_{j\mathbf{k}}(\mathbf{r}) = \sum_{\mathbf{R}} e^{i\mathbf{k}\cdot\mathbf{R}}\,w_j(\mathbf{r}-\mathbf{R}) \tag{10}$$

where $w_j(\mathbf{r}-\mathbf{R})$ is the j'th Wannier function in unit cell $\mathbf{R}$. Then the spillage is again computed using Eqs. (4) and (9). This will be accurate as long as the WFs for the systems with and without SOC are chosen to be the same, or as similar as possible. As we shall see in the following section, the results from the Wannier basis match those of the direct plane-wave calculation very closely for the cases studied here.

In the case of complex unit cells or supercells with many bands near the gap, it may be difficult to identify precisely

which bands have been inverted by the SOC. In this case it may be helpful to define a valence-band-resolved spillage as $\gamma_n(\mathbf{k}) = [L(\mathbf{k})L^\dagger(\mathbf{k})]_{nn}$, where $L_{nm}(\mathbf{k}) = \langle\psi_{n\mathbf{k}}|\tilde{\psi}_{m\mathbf{k}}\rangle$ is the overlap matrix between the occupied states without SOC and the unoccupied states with SOC. Then the total spillage is $\gamma(\mathbf{k}) = \sum_{n=1}^{n_{\rm occ}} \gamma_n(\mathbf{k})$. Similarly, $\bar{\gamma}_m = (L^\dagger L)_{mm}$ provides a conduction-band-resolved spillage. However, it should be noted that γ_n and $\bar{\gamma}_m$ are not gauge-invariant; they will change under a unitary transformation among the occupied or unoccupied states. A natural gauge choice is the one associated with the singular-value decomposition $L = V\Sigma W^\dagger$. Transforming the sets of occupied and unoccupied states according to the unitary matrices V and W respectively, the overlap matrix between the transformed states is just Σ, which is real and diagonal. The columns of V (W) corresponding to the leading eigenvalues indicate which linear combinations of valence (conduction) states contribute the most to the total spillage. We leave the exploration of these refinements for a future study.

B. Relation to topological character

Here we argue that the presence of non-trivial topological indices will be reflected in certain features of the spillage distribution in the BZ.

We first consider the relatively simple case in which the SOC-driven band inversion is associated with the crossing of highest valence and lowest conduction states belonging to two different irreducible representations (irreps) at a high-symmetry point $\mathbf{k} = \Lambda_0$ in the BZ. Since the states belonging to different irreps have no overlap with each other, the spillage at Λ_0 must be greater than or equal to the irrep dimension. In TR-invariant Bi_2Se_3, for example, the four states around the Fermi level at Γ consist of two Kramers doublets of opposite parity. In this case the dimension of the irreps is two, so we expect a peak in $\gamma(\mathbf{k})$ centered at Γ whose height is $\gamma_{\max} \geq 2$. As we shall show in Sec. III D, this is exactly what we find in Bi_2Se_3.

Next, we argue that a correspondence between topological character and spillage should also remain valid for more general cases without special lattice symmetry. Let us first consider the case of CIs (i.e., with broken TR symmetry). We assume the Bloch functions $\psi_{n\mathbf{k}}$ are those of a normal system with Chern number $C = 0$, while $\tilde{\psi}_{n\mathbf{k}}$ are topologically non-trivial with a nonzero Chern number $\widetilde{C}$. We argue that this implies the existence of at least one point in the BZ where the spillage is ≥ 1. If we assume the contrary, i.e., $\gamma(\mathbf{k}) < 1$ everywhere in the BZ, then the determinant of the overlap matrix of Eq. (5) between $\psi_{n\mathbf{k}}$ and $\tilde{\psi}_{n\mathbf{k}}$ obeys $\det(M_{\mathbf{k}}) > 0$ everywhere, since a singular M would imply $\gamma \geq 1$. Because the system $|\psi_{n\mathbf{k}}\rangle$ is topologically normal, we know it is possible to choose a smooth and periodic gauge for it, and we assume without loss of generality that this has been done. But if $M_{\mathbf{k}}$ is nowhere singular, the $|\psi_{n\mathbf{k}}\rangle$ can be used as "trial functions" to construct a smooth and periodic gauge for the $|\tilde{\psi}_{n\mathbf{k}}\rangle$, as follows. At each $\mathbf{k}$, carry out a singular value decomposition to express $M = V^\dagger\Sigma W$ (V and W are unitary and Σ is real positive diagonal), and then use the unitary matrix $V^\dagger W$ to transform the original $\tilde{\psi}_{n\mathbf{k}}$ to a new set $\tilde{\psi}'_{n\mathbf{k}}$. Then $M = V^\dagger\Sigma V$, i.e., it is Hermitian and positive definite. Intuitively, this means that a smooth and periodic gauge has been chosen for the states $\tilde{\psi}'_{n\mathbf{k}}$ to make them "maximally aligned" with the states $\psi_{n\mathbf{k}}$. But a smooth and periodic gauge is inconsistent with a nonzero Chern number, completing the proof by contradiction. Thus, if $\gamma < 1$ everywhere in the BZ, then $M_{mn,\mathbf{k}}$ is nonsingular everywhere, and the system $|\tilde{\psi}_{n\mathbf{k}}\rangle$ is normal. Conversely, a topological system must have $\gamma(\mathbf{k}) \geq 1$ somewhere in the BZ, which provides both a signal for the topological phase and an indication of where in the BZ the band inversion has occurred.

For the TR-invariant $\mathbb{Z}_2$ TIs, similar arguments can be put forward that work even in the absence of inversion symmetry. If the system of $|\psi_{n\mathbf{k}}\rangle$ is in the $\mathbb{Z}_2$-even phase, one can always make a smooth gauge choice over the entire BZ that respects TR symmetry. In the $\mathbb{Z}_2$-odd case, however, such a gauge choice does not exist.[24,25] Therefore, $\det(M_{\mathbf{k}})$ must vanish somewhere in BZ, or else the smooth gauge could be transferred to the $|\tilde{\psi}_{n\mathbf{k}}\rangle$, resulting in a contradiction. Due to the TR symmetry, $\det(M_{\mathbf{k}}) = \det(M_{-\mathbf{k}})$, so one would generically expect $\gamma(\mathbf{k}) \geq 1$ at two points ($\mathbf{k}_0$ and $-\mathbf{k}_0$) in the BZ. For the case of inversion-symmetric TIs, $\mathbf{k}_0$ and $-\mathbf{k}_0$ merge at one of the TRIM, the two spillages add up, and one expects $\gamma \geq 2$ at one of the TRIM.

In the following section, we numerically test and confirm the above arguments by applying the formalism to systems in different topological phases.

III. APPLICATIONS

A. Application to two-band Dirac Hamiltonian

As a warm-up exercise, we first apply the spillage formula to a minimal model of a band inversion in 2D (k_x, k_y) space, namely a Dirac model at half filling as described by the Hamiltonian

$$H = m(1-\lambda)\sigma_z + k_x\sigma_x + k_y\sigma_y \tag{11}$$

where σ_j are Pauli matrices. Here m is a mass and λ is a control parameter that inverts the bands at $\lambda = 1$. Physically, such a model may describe the low-energy physics in the vicinity of a band touching event associated with the transition from a normal to a quantum anomalous Hall insulator, or at one of the band touching events (at $\mathbf{k}_0$ or $-\mathbf{k}_0$) in the transition to a spin-Hall insulator. The energy spectrum of the above Hamiltonian is $E_\pm = \pm\sqrt{m^2(1-\lambda)^2 + k_x^2 + k_y^2}$, where the gap closes at $\lambda = 1$ at Γ ($k_x = k_y = 0$). The spillage is just $\gamma(\lambda, \mathbf{k}) = 1 - |\langle\psi^0_{1\mathbf{k}}|\psi^\lambda_{1\mathbf{k}}\rangle|^2$, where $|\psi^0_{1\mathbf{k}}\rangle$ ($|\psi^\lambda_{1\mathbf{k}}\rangle$) is the occupied eigenstate at zero (non-zero) λ.

Figure 1 shows the spillage *vs.* k_x at $k_y = 0$ as λ is increased from 0.4 to 1.9. When $\lambda = 0.4$, the spillage is negligible almost everywhere, and is exactly zero at Γ. On the other hand, when $\lambda = 0.99$, which is very close to the gap closure point, one finds two peaks of spillage emerging on either side of Γ,

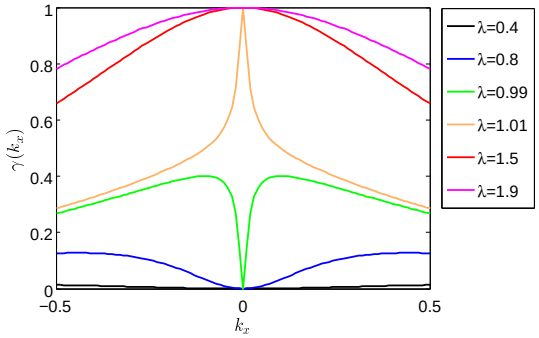

FIG. 1. The spillage of the half-filled Dirac Hamiltonian as λ increases from 0.4 to 1.9.

with a peak value approaching 0.5 as $\lambda \to 1$. As λ passes through the critical point at $\lambda = 1$, one finds that the spillage at Γ jumps from 0 to 1, and then gradually spreads out in BZ as λ is increased further.

This interesting behavior can be interpreted as follows. When $\lambda = 0$, the σ_z term dominates around Γ, so that the pesudospin is mostly along the z direction around Γ. On the other hand, if λ is very close to 1, the σ_x and σ_y terms dominate near (but not exactly at) Γ, forcing the pseudospin direction to point in the (x, y) plane and resulting in a spillage of 1/2. However, the σ_x and σ_y terms vanish at Γ, which means the pseudospin has to point along the $\pm z$ direction. Therefore, when $\lambda < 1$ ($\lambda > 1$), the pseudospin is parallel (anti-parallel) with the pseudospin direction at $\lambda = 0$, such that the spillage jumps from 0 to 1 as λ passes through the critical point.

B. Application to the Kane-Mele model

The Kane-Mele model is a four-band TB model on a graphene lattice, including nearest-neighbor (NN) spin-independent hoppings and both NN and next-NN spin-dependent hoppings:

$$H = \sum_{\langle ij\rangle} t c_i^\dagger c_j + \sum_{\langle\langle ij\rangle\rangle} i\lambda_{\rm so}\nu_{ij} c_i^\dagger s_z c_j + \sum_{\langle ij\rangle} i\lambda_{\rm R} c_i^\dagger (\mathbf{s}\times\hat{\mathbf{d}}_{ij})_z c_j + \sum_i \epsilon(-1)^i c_i^\dagger c_i \,. \quad (12)$$

Here spin is implicit, t is the NN spin-independent hopping amplitude, $\lambda_{\rm so}$ is the strength of the next-NN non-spin-flip SOC, $\lambda_{\rm R}$ is the NN Rashba-like SOC amplitude, and ϵ is the magnitude of on-site energy, with signs ± 1 for A and B sublattices respectively. Also, $\nu_{ij} = \pm 1$ with the sign depending on the chirality of the next-NN bond from site i to j, and $\hat{\mathbf{d}}_{ij}$ is the unit vector pointing from site i to its NN j. In this model, $\lambda_{\rm so}$ competes with $\lambda_{\rm R}$ and ϵ, in the sense that $\lambda_{\rm so}$ tends to drive the system to the QSH phase while $\lambda_{\rm R}$ and ϵ tend to retain the trivial band topology.

For simplicity, we first drop the Rashba coupling, so that spin is a good quantum number. The system is in the QSH phase when $3\sqrt{3}\lambda_{\rm so} > \epsilon$, and in the normal phase otherwise. Without the Rashba term, the Kane-Mele model can

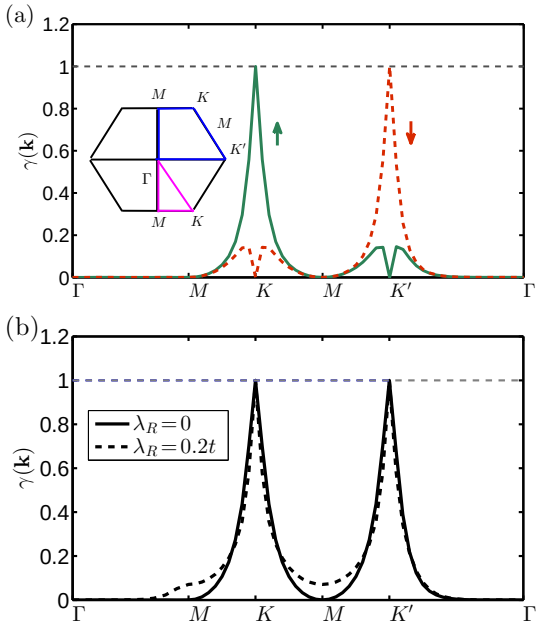

FIG. 2. Spin-orbit spillage of the Kane-Mele model in the QSH phase, with $t = 1$, $\lambda_{\rm so} = 0.1t$, and $\epsilon = 0.1t$. (a) Spin-resolved spillage without Rashba coupling; solid (green) and dashed (red) lines denote spin-up and spin-down spillage. Inset shows Γ-M-K-M-K′-Γ path used here (blue) and K-Γ-M-K path used in Fig. 3 (magenta). (b) Total spillage without (solid line) and with (dashed line) Rashba coupling.

be considered as a superposition of two copies of the Haldane model with opposite Chern numbers.[15] If one calculates the 2D Chern numbers for spin-up and spin-down electrons separately, one would find that the two Chern numbers are ± 1 in the QSH phase. While the Haldane-model system goes from a normal insulator to a CI via a band inversion at either the K or K′ point, the Kane-Mele model transitions to the QSH state via simultaneous band inversions at both K and K′, but for opposite spins at these two points.

The SOC-induced spillage without the Rashba term is shown in Fig. 2(a). In this case the spins act independently, so the spin-up and spin-down spillages $\gamma_\sigma(\mathbf{k}) = n_{\rm occ}/2 - \sum_{m,n=1}^{n_{\rm occ}/2} |M_{n\sigma,m\sigma}(\mathbf{k})|^2$ (where $\sigma = \{\uparrow,\downarrow\}$) are shown separately. Clearly the spin-up band inversion at K is responsible for $\gamma_\uparrow = 1$, and conversely at K′. The total spillage $\gamma(\mathbf{k}) = \gamma_\uparrow(\mathbf{k}) + \gamma_\downarrow(\mathbf{k})$ is shown by the solid line in Fig. 2(b). The symmetry between the behavior at K and K′ has been restored by summing over spins. Note that the peak values are $\gamma = 1$ exactly; the fact that they do not exceed one is an artifact of the simplicity of the model. It is also interesting to note that in the absence of time-reversal symmetry, the spin-resolved spillage is closely related to the van Vleck paramagnetism in spin-orbit coupled systems.

When the Rashba coupling is included, as shown by the dashed line in Fig. 2(b), spin is no longer a good quantum number, so that a spin decomposition is not well-defined. As expected, adding the Rashba term does not significantly change the results;[26] one still finds that the spillage reaches

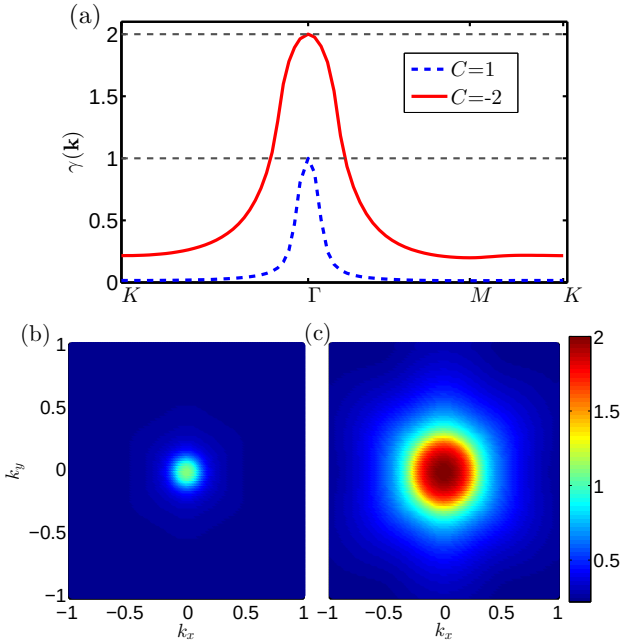

FIG. 3. (a) Spin-orbit spillage of the Bi bilayer for $C = 1$ (dashed blue) and $C = -2$ (solid red) phases, plotted along the K-Γ-M-K path (magenta path in inset of Fig. 2(a)). (b) Spillage for $C = 1$ phase plotted in the 2D BZ (k_x and k_y in units of Å^{-1}). (c) Same for $C = -2$ phase.

unity at K and K′ as before, providing an indication of the spin-Hall phase.

C. Application to Chern insulators

We now consider the case of broken TR symmetry, so that the $\mathbb{Z}_2$ index is no longer well-defined, but the possibility of CI phases appears. As discussed in Sec. I, SOC is important here as well. Here we study a buckled honeycomb Bi bilayer with a Zeeman field applied normal to the plane, which can be regarded as having been cut from a 3D Bi crystal on a (111) plane. The Bi (111) bilayer has been proposed as a candidate for QSH insulator.[27] If a Zeeman field is further applied, it is possible to obtain CI phases with Chern numbers $C = 1$ or $C = -2$.[16,28] To describe this system we use a TB model based on Bi $6s$ and $6p$ orbitals, where the first-neighbor ss, sp, $pp\sigma$, and $pp\pi$ hoppings, as well as the second-neighbor $pp\sigma$ hoppings, are included. The hopping parameters are taken from a TB model for 3D bulk Bi.[29] In order to obtain non-zero Chern numbers, an on-site p-shell SOC ($\lambda_{\rm SOC}$) and a Zeeman field (H_z) are further applied. It turns out that if H_z is fixed at 0.8 eV, then the phases with $C = -2$ and $+1$ are realized at $\lambda_{\rm SOC} = 2.4$ eV and 0.6 eV respectively. If the SOC is completely turned off, $C = 0$.

The spillage for the Bi bilayer is shown along a high-symmetry k-path in Fig. 3(a), and as a distribution in the 2D BZ in Figs. 3(b-c), for the two parameter sets giving the $C = 1$ and $C = -2$ phases. In both cases the spillage distribution is concentrated at Γ, indicating a band inversion there, although

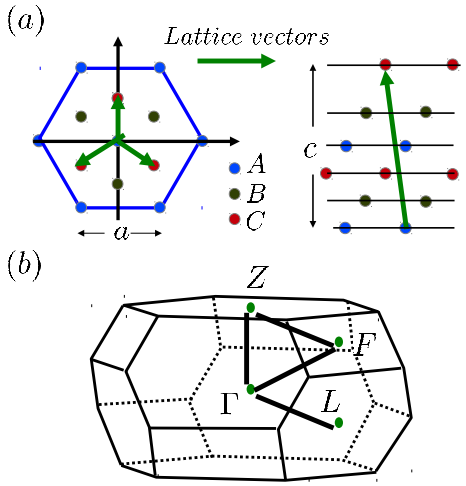

FIG. 4. (a) Lattice structure of Bi_2Se_3. (b) The BZ of Bi_2Se_3; the spillage and bandstructures shown in Fig. 5(a) and Fig. 6 are plotted along the black path.

it is much more sharply peaked in the $C = 1$ case. Clearly the spillages provide a signature of the presence of a Chern-insulator phase, including the location of the band inversion and the magnitude (but not the sign) of the Chern number. Here again the peak values of the spillage are exactly equal to the magnitude of the Chern number. For more realistic systems with more bands included, the spillage can be expected to exceed these values slightly, but a clear correlation between the peak values of spillage and the Chern number is still expected.

D. Application to 3D topological insulators

In this subsection we apply our formalism to realistic first-principles calculations of Bi_2Se_3, In_2Se_3 and Sb_2Se_3. Bi_2Se_3 is a well-known strong TI,[13] where the SOC-induced band inversion takes place at Γ. We also consider In_2Se_3 and Sb_2Se_3 in the same crystal structure (known as β phase for In_2Se_3 and not realized experimentally for Sb_2Se_3), which are theoretically predicted (and experimentally confirmed for In_2Se_3) to be trivial insulators.[13,30–32] Here it is interesting to note that even though Sb and In have very similar atomic SOC strength, the substitution of In atoms tends to drive Bi_2Se_3into a trivial-insulator phase much faster than does Sb substitution, due to the existence of In $5s$ orbitals.[32]

As shown in Fig. 4, the considered structure is rhombohedral, with two cations and three Se atoms in the primitive unit cell. The five 2D monolayers are stacked in an A-B-C-A-... sequence along the (111) direction to form quintuple layers (QLs). Experimentally the in-plane hexagonal parameters are $a = 4.138$ and 4.05 Å, and the QL size is $c = 9.547$ and 9.803 Å, for Bi_2Se_3 and In_2Se_3 respectively. In our calculations, we take the experimental lattice parameters of Bi_2Se_3 and In_2Se_3, but relax their internal atomic coordinates. As for Sb_2Se_3, because its rhombohedral structure is not adopted in nature, both the lattice parameters and atomic positions are re-

laxed. The ground state of rhombohedral Sb_2Se_3 is predicted to be a trivial insulator with $a = 4.11$ Å and $c = 10.43$ Å.

We use the QUANTUM ESPRESSO package[33] to carry out first-principles calculations on these systems both with and without SOC. The PBE generalized-gradient approximation (GGA) is taken to treat the exchange-correlation functional,[34,35] and norm-conserving pseudopotentials are generated from OPIUM package.[36,37] The energy cutoff is taken as 65 Ry for In_2Se_3 and 55 Ry for Bi_2Se_3 and Sb_2Se_3, with an $8\times8\times8$ Monkhorst-Pack $\mathbf{k}$ mesh.[38] The wavefunctions defined in the plane-wave basis are extracted from these calculations and Eq. (6) is applied to evaluate the spillage.

As mentioned in Sec. I, the spillage can also be calculated in the Wannier basis. Starting from the first-principles calculations, we use the WANNIER90 package[39] to construct Wannier functions (WFs) and a corresponding realistic TB model[40] for each of the three materials. The basis WFs are constructed by projecting 30 atomic p trial orbitals onto the Bloch subspace of p-like bands to generate a 30-band spinor model for Bi_2Se_3 and Sb_2Se_3, whereas four additional In $5s$ projectors and bands are included in the model for In_2Se_3. In order that they will retain their atomic-like identity as much as possible, the projected WFs are not optimized to minimize the spread functional.[23] We find that the WFs generated by this projection method are almost the same for the systems with and without SOC, so that the matrix elements $M_{mn}(\mathbf{k})$ defined in Sec. II A can be evaluated with good accuracy.

The spillage from the direct plane-wave calculations are shown as the solid lines in Fig. 5(a). For Bi_2Se_3, the spillage $\gamma(\mathbf{k})$ has a peak value of 2.12 at Γ, which is slightly larger than 2, indicating that two Kramers degenerate bands at Γ have been inverted by SOC. On the other hand, the effect of SOC in In_2Se_3 and Sb_2Se_3 seems to be negligible everywhere in the BZ, which is consistent with the fact that they are both trivial insulators.

The calculations carried out in the Wannier basis are shown by the dashed lines in Fig. 5(a). The spillage is typically slightly larger for the direct plane-wave calculations, since the fact that the WFs have a slightly different plane-wave representation with and without SOC is not taken into account in the Wannier-based calculations. Still, the qualitative features are the same, showing that the Wannier-based approach can successfully provide the same kind of information about the nature and location of the topological band inversion. In Fig. 5(b) we also show the spillage of Bi_2Se_3 in the (k_x, k_y) plane at $k_z = 0$, as calculated in the Wannier basis, which again indicates a highly localized band inversion near Γ and is fully consistent with the expected picture of the band inversion in Bi_2Se_3.

To see the band inversion from another perspective, we plot in Fig. 6 the bulk bandstructures of Sb_2Se_3 and Bi_2Se_3 projected onto Sb $5p$ and Bi $6p$ orbitals respectively. It is clear that for Sb_2Se_3, the Sb $5p$ orbitals are almost all concentrated in the conduction bands, whereas in Bi_2Se_3 there is a localized region around Γ where the corresponding Bi $6p$ orbitals contribute mostly to the top valence band. This is precisely the region of the band inversion corresponding to the peak at Γ in Fig. 5.

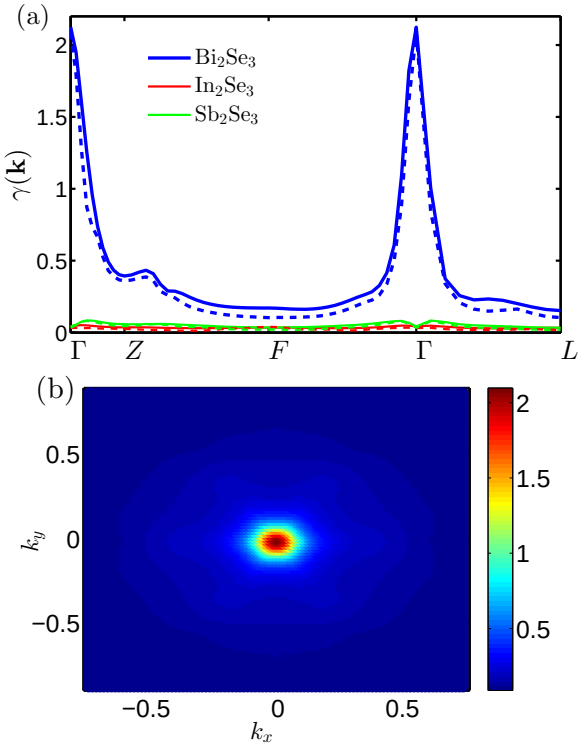

FIG. 5. (a) Spin-orbit spillage of rhombohedral Bi_2Se_3, Sb_2Se_3 and In_2Se_3 as indicated by blue, green and red lines respectively. Solid (dashed) lines show the spillage computed from direct plane-wave (Wannier-based) calculations. (b) Spillage of Bi_2Se_3 in the (k_x, k_y) plane at $k_z = 0$ (units of Å^{-1}).

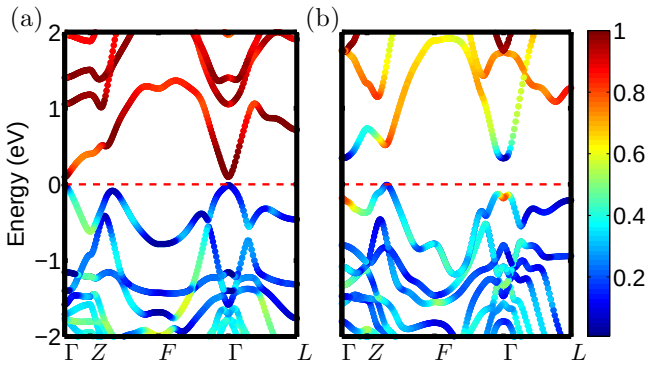

FIG. 6. (a) Wannier-interpolated bandstructure of Sb_2Se_3. (b) Same for Bi_2Se_3. Color coding indicates weight of Sb $5p$ or Bi $6p$ orbitals.

IV. SUMMARY

To summarize, we have introduced the SOC-induced spillage $\gamma(\mathbf{k})$ as a useful quantitative tool for evaluating the degree of band inversion driven by SOC and mapping it as a function of $\mathbf{k}$ in the BZ. We have applied this method to the two-band Dirac model, the 2D Kane-Mele model and a tight-binding model of a Bi bilayer with applied Zeeman field, as well as to realistic materials including both trivial and topological insulators. A clear correspondence between non-trivial

topological indices and non-trivial spillage distributions is evident. In the two-band Dirac model, one observes interesting behavior in the distribution of spillage through a topological phase transition process. In the Kane-Mele model, one gets two peaks of spillage at K and K′ with the peak value of 1, which indicates that a single band is inverted at these two points corresponding to an odd 2D $\mathbb{Z}_2$ index. In the Bi bilayer with applied Zeeman field, a peak of spillage shows up at Γ, with the peak value corresponding to the absolute value of the Chern number. In Bi_2Se_3, the spillage is slightly greater than 2 at one of the TRIM, namely Γ, implying that two bands are inverted by SOC there and signaling the presence of a nontrivial strong $\mathbb{Z}_2$ index.

As mentioned above, other methods exist for the direct computation of topological Chern and $\mathbb{Z}_2$ indices, with or without inversion symmetry,[14,41,42] and we still recommend these if a direct and definitive determination of the topological indices is needed. However, the present spillage-based approach has the advantage of providing a BZ map of the strength, position, and degree of localization of the band inversion responsible for the topological character, thus giving valuable physical intuition about the origin of the topological properties of the material in question. In addition, compared with direct methods for topological index calculation, the spillage calculation only requires the evaluation of overlaps between two wavefunctions at the same $\mathbf{k}$ point, which is easy to implement and numerically very efficient. Therefore, it is our hope that the calculation of SOC spillage will prove to be a widely useful tool that can be applied both for high-throughput screening for topological materials and for obtaining a deeper understanding of the critical features of the bandstructures in known topological materials.

ACKNOWLEDGMENTS

This work was supported by NSF Grant DMR-10-05838. We appreciate valuable discussions with Hongbin Zhang and Huaqing Huang.

[1] R. Winkler, *Spin-orbit coupling effects in two-dimensional electron and hole systems*, Vol. 191 (Springer Verlag, 2003)

[2] B. Nikolić, L. Zarbo, and S. Souma, *The Oxford Handbook on Nanoscience and Technology: Frontiers and Advances* (Oxford University Press, 2010) edited by A. V. Narlikar and Y. Y. Fu, Vol. I, Chap. 24, pp. 814866

[3] M. V. Berry, Proceedings of the Royal Society of London. A. Mathematical and Physical Sciences **392**, 45 (1984)

[4] S. Hikami, A. I. Larkin, and Y. Nagaoka, Progress of Theoretical Physics **63**, 707 (1980)

[5] J. E. Hirsch, Phys. Rev. Lett. **83**, 1834 (Aug 1999)

[6] B. A. Bernevig, T. L. Hughes, and S.-C. Zhang, Science **314**, 1757 (2006)

[7] M. König, S. Wiedmann, C. Brüne, A. Roth, H. Buhmann, L. W. Molenkamp, X.-L. Qi, and S.-C. Zhang, Science **318**, 766 (2007)

[8] C. L. Kane and E. J. Mele, Phys. Rev. Lett. **95**, 146802 (2005)

[9] C. L. Kane and E. J. Mele, Phys. Rev. Lett. **95**, 226801 (2005)

[10] M. Z. Hasan and C. L. Kane, Rev. Mod. Phys. **82**, 3045 (Nov 2010)

[11] X.-L. Qi and S.-C. Zhang, Rev. Mod. Phys. **83**, 1057 (Oct 2011)

[12] W. Feng and Y. Yao, Science China Physics, Mechanics and Astronomy **55**, 2199 (2012)

[13] H. Zhang, C.-X. Liu, X.-L. Qi, X. Dai, Z. Fang, and S.-C. Zhang, Nature Physics **5**, 438 (2009)

[14] L. Fu and C. L. Kane, Phys. Rev. B **76**, 045302 (2007)

[15] F. D. M. Haldane, Phys. Rev. Lett. **61**, 2015 (Oct 1988)

[16] H. Zhang, F. Freimuth, G. Bihlmayer, M. Ležaić, S. Blügel, and Y. Mokrousov, Phys. Rev. B **87**, 205132 (May 2013)

[17] M. Klintenberg, arXiv:1007.4838(2010)

[18] K. Yang, W. Setyawan, S. Wang, M. B. Nardelli, and S. Curtarolo, Nature Materials **11**, 614 (2012)

[19] P. Hohenberg and W. Kohn, Phys. Rev. **136**, B864 (Nov 1964)

[20] W. Kohn and L. J. Sham, Phys. Rev. **140**, A1133 (Nov 1965)

[21] I. Souza, N. Marzari, and D. Vanderbilt, Phys. Rev. B **65**, 035109 (2001)

[22] J. R. Yates, X. J. Wang, D. Vanderbilt, and I. Souza, Phys. Rev. B **75**, 195121 (2007)

[23] N. Marzari, A. A. Mostofi, J. R. Yates, I. Souza, and D. Vanderbilt, Rev. Mod. Phys. **84**, 1419 (Oct 2012)

[24] L. Fu and C. L. Kane, Phys. Rev. B **74**, 195312 (2006)

[25] A. A. Soluyanov and D. Vanderbilt, Phys. Rev. B **85**, 115415 (Mar 2012)

[26] The $\mathbf{k}$-dependence of the Rashba coupling terms is such that they vanish at K and K′.

[27] S. Murakami, Phys. Rev. Lett. **97**, 236805 (Dec 2006)

[28] H. Zhang, F. Freimuth, G. Bihlmayer, S. Blügel, and Y. Mokrousov, Phys. Rev. B **86**, 035104 (Jul 2012)

[29] Y. Liu and R. E. Allen, Phys. Rev. B **52**, 1566 (Jul 1995)

[30] M. Brahlek, N. Bansal, N. Koirala, S.-Y. Xu, M. Neupane, C. Liu, M. Z. Hasan, and S. Oh, Phys. Rev. Lett. **109**, 186403 (Oct 2012)

[31] L. Wu, M. Brahlek, R. V. Aguilar, A. Stier, C. Morris, Y. Lubashevsky, L. Bilbro, N. Bansal, S. Oh, and N. Armitage, Nature Physics **9**, 410 (2013)

[32] J. Liu and D. Vanderbilt, Phys. Rev. B **88**, 224202 (Dec 2013)

[33] P. Giannozzi, S. Baroni, N. Bonini, M. Calandra, R. Car, C. Cavazzoni, D. Ceresoli, G. L. Chiarotti, M. Cococcioni, I. Dabo, A. Dal Corso, S. de Gironcoli, S. Fabris, G. Fratesi, R. Gebauer, U. Gerstmann, C. Gougoussis, A. Kokalj, M. Lazzeri, L. Martin-Samos, N. Marzari, F. Mauri, R. Mazzarello, S. Paolini, A. Pasquarello, L. Paulatto, C. Sbraccia, S. Scandolo, G. Sclauzero, A. P. Seitsonen, A. Smogunov, P. Umari, and R. M. Wentzcovitch, Journal of Physics: Condensed Matter **21**, 395502 (19pp) (2009)

[34] J. P. Perdew, K. Burke, and M. Ernzerhof, Phys. Rev. Lett. **77**, 3865 (Oct 1996)

[35] J. P. Perdew, K. Burke, and M. Ernzerhof, Phys. Rev. Lett. **78**, 1396 (Feb 1997)

[36] `http://opium.sourceforge.net/`

[37] N. J. Ramer and A. M. Rappe, Phys. Rev. B **59**, 12471 (May 1999)

[38] H. J. Monkhorst and J. D. Pack, Phys. Rev. B **13**, 5188 (Jun 1976)

[39] A. A. Mostofi, J. R. Yates, Y. S. Lee, I. Souza, D. Vanderbilt, and N. Marzari, Computer Phys. Comm. **178**, 685 (2008)

[40] The TB models from Wannier90 are constructed in such a way that the Wannier-interpolated bandstructure reproduces the first-principles bandstructure exactly within an energy window cen-

tered around the Fermi level.

[41] T. Fukui, Y. Hatsugai, and H. Suzuki, Journal of the Physical Society of Japan **74**, 1674 (2005)
[42] A. A. Soluyanov and D. Vanderbilt, Phys. Rev. B **83**, 235401 (JUN 2 2011), ISSN 1098-0121